

## 1 STUDY SITE

1 The Guttannen (GT) site in the Bern region lies at 1047 m a.s.l.. In the winter (Oct-Apr), mean daily  
 2 minimum and maximum air temperatures vary between -13 and 15 °C. Clear skies are rare, averaging  
 3 around 7 days during winter (Meteoblue, 2020). The site was situated adjacent to a stream resulting in high  
 4 humidity values across the study period. An automatic weather station (AWS) was adjacent to the wooden  
 5 boundary as shown in Fig. ???. The fountain used for spraying water had a height of 1.35 m, and was placed  
 6 in the centre of the wooden enclosure. The water was transferred from a spring water source and flowed via  
 7 a flowmeter and an air escape valve to the nozzle. The air escape valve was installed to avoid errors in the  
 8 flow measurements due to air bubbles. In addition, a webcam guaranteed a continuous survey of the site  
 9 during the construction of the Icestupa.

### 10 1.1 Measurements and Data

11 Measurements comprising air temperature, relative humidity, water flow rate, wind speed and direction  
 12 were made every 5 minutes throughout the construction period. The water flow rate or discharge was  
 13 measured via an ultrasonic sensor attached to the fountain supply pipeline.

14 In addition, we used ERA5 reanalysis dataset (Copernicus Climate Change Service (C3S), 2017) for  
 15 filling data gaps and adding data that were not measured directly at the EP site. The 2 m temperature  
 16 parameter correlated with air temperature ( $r^2 = 0.9$ ), surface pressure parameter correlated with air  
 17 pressure ( $r^2 = 1$ ) and 10m wind speed parameter (derived from horizontal and vertical components)  
 18 correlated with wind speed ( $r^2 = 0.6$ ). The ERA5 reanalysis dataset has a good correlation with lower  
 19 elevation sites in Switzerland (Scherrer, 2020). The hourly ERA5 data and the 10 minute Plaffeien AWS  
 20 data were linearly interpolated to the 5 minute data frequency of the EP AWS.

21 The ERA5 grid point chosen (Latitude 46° 38' 24" N, Longitude 7° 14' 24" E) for the EP site was around  
 22 9 km away from the actual site. All the ERA5 variables were therefore fitted with the EP dataset via linear  
 23 regressions.

#### 24 1.1.1 Drone Measurements for calibration and validation

25 Several Drone flights were conducted in every AIR site. The DEM generated through these flights were  
 26 analysed to obtain the circumference and volume of the ice structure. The mean circumference measured  
 27 during the fountain duration was set as the spray radius ( $r_{spray}$ ) and the volume obtained in the first drone  
 28 flight was set as the dome volume ( $V_{dome}$ ) for model initialisation.

29

Name	Location	Shortname	Fountain duration	Spray radius
Icestupa Competition 2021	Gangles, India	IC21	Jan 18 - Mar 10	10.8m
Guttannen Bewegt 2021	Guttannen, Switzerland	GB21	Nov 22 - Feb 21	6.9 m
Guttannen Bewegt 2020	Guttannen, Switzerland	GB20	Jan 3 - Feb 27	7.7 m
Eispalast 2019	Schwarzsee, Switzerland	EP19	Jan 30 - Feb 16	1.2 m

## 2 MODEL SETUP

31 A bulk energy and mass balance model is used to calculate the amounts of ice, meltwater, water vapour  
 32 and runoff water of the AIR every hour. This model consists of four modules which estimates the AIR, a)  
 33 geometric evolution , b) energy balance, c) surface temperature and d) mass balance.

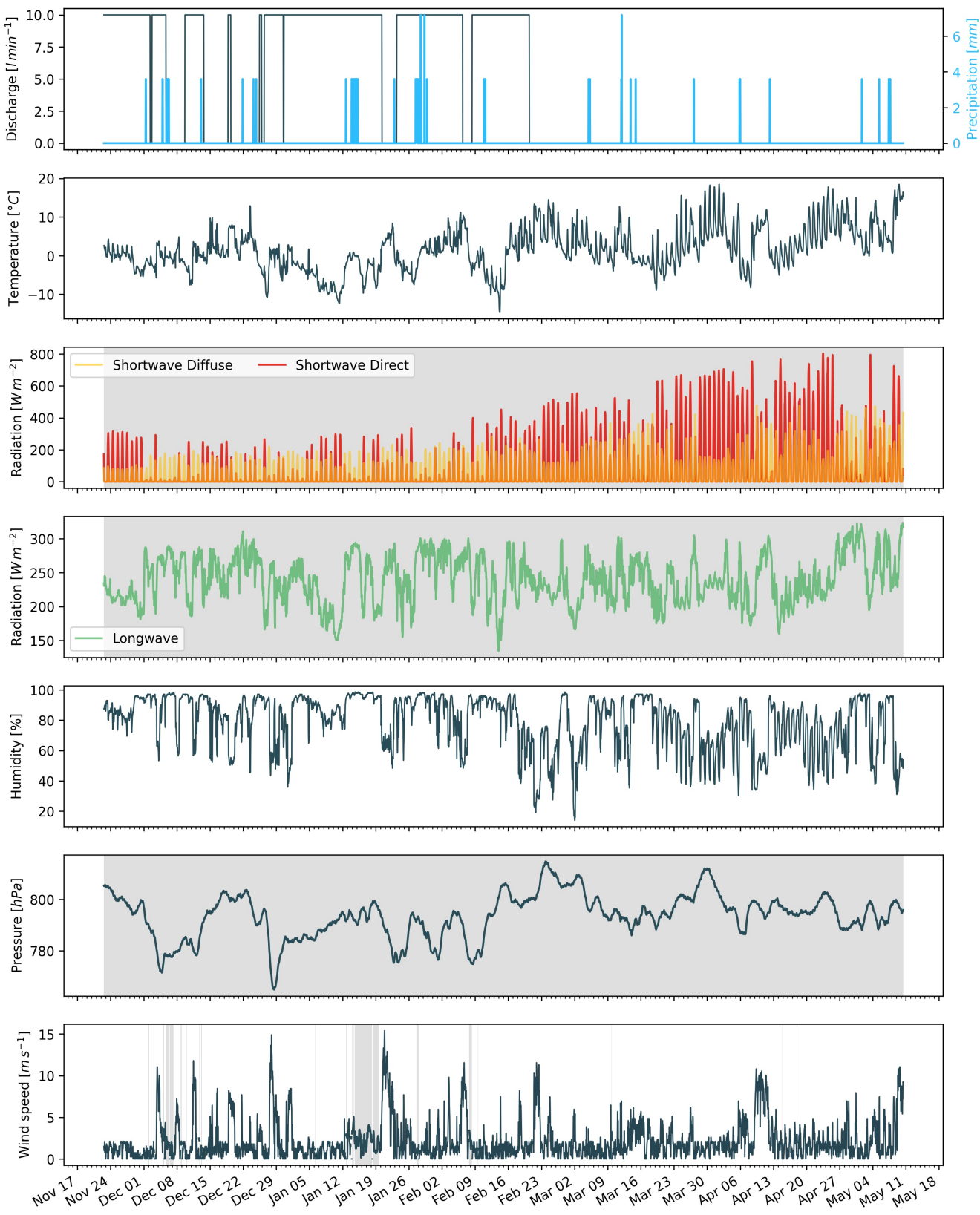


**Figure 1.** Measurements at the AWS of GB21 were used as main model input data in hourly frequency. Missing data, data gaps and errors were filled from the ERA5 dataset (shaded regions).

34 **2.1 Geometric evolution**

35 Radius  $r_{ice}^i$  and height  $h_{ice}^i$  define the dimensions of the AIR assuming its geometry to be a cone. The  
36 surface area  $A^i$  exposed to the atmosphere and volume  $V^i$  are:

$$A = \pi \cdot r_{ice} \cdot \sqrt{r_{ice}^2 + h_{ice}^2} \quad (1)$$

$$V = \frac{\pi}{3} \cdot r_{ice}^2 \cdot h_{ice} \quad (2)$$

37 Note that we do not specify the time step superscript  $i$  of the shape variables  $A$ ,  $V$ ,  $r_{ice}$  and  $h_{ice}$  for  
38 brevity. The equations used henceforth display model time step superscript  $i$  only if it is different from the  
39 current time step.

40 With the mass of the AIR  $M_{ice}$ , its current volume can also be expressed as:

$$V = M_{ice} / \rho_{ice} \quad (3)$$

41 where  $\rho_{ice}$  is the density of ice ( $917 \text{ kg m}^{-3}$ ).

42 The influence of the AIR fountain is parameterised by the fountain water temperature  $T_w$  and its spray  
43 radius  $r_{spray}$ . The initial radius  $r_0$  of the AIR is assumed to be  $r_{spray}$ . The initial height  $h_0$  depends on the  
44 dome volume  $V_{dome}$  used to construct the AIR as follows:

$$h_0 = \Delta x + \frac{3 \cdot V_{dome}}{\pi r_{spray}^2} \quad (4)$$

45 where  $\Delta x$  is the surface layer thickness (defined in Section 2.2)

46 During subsequent time steps, the dimensions of the AIR evolve assuming a uniform ice formation and  
47 decay across its surface area with an invariant slope  $s_{cone} = \frac{h_{ice}}{r_{ice}}$ . During these time steps, the volume is  
48 parameterised using Eqn. 2 as:

$$V = \frac{\pi \cdot r_{ice}^3 \cdot s_{cone}}{3} \quad (5)$$

49 However, the Icestupa cannot outgrow the maximum range of the water droplets ( $(r_{ice})_{max} = r_F$ ).  
50 Combining equations 2, 4, 3 and 5, the geometric evolution of the Icestupa at each time step  $i$  can be  
51 determined by considering the following rules:

$$(r_{ice}, h_{ice}) = \begin{cases} (r_{spray}, h_0) & \text{if } i = 0 \\ (r_{ice}^{i-1}, \frac{3 \cdot M_{ice}}{\pi \cdot \rho_{ice} \cdot (r_{ice}^{i-1})^2}) & \text{if } r_{ice}^{i-1} \geq r_F \text{ and } \Delta M_{ice} > 0 \\ (\frac{3 \cdot M_{ice}}{\pi \cdot \rho_{ice} \cdot s_{cone}})^{1/3} \cdot (1, s_{cone}) & \text{otherwise} \end{cases} \quad (6)$$

52 where  $\Delta M_{ice} = M_{ice}^{i-1} - M_{ice}^{i-2}$

53 **2.2 Energy Balance**

54 The energy balance equation (Hock, 2005) for the AIR is formulated as follows:

$$q_{SW} + q_{LW} + q_L + q_S + q_F + q_G = q_{surf} \quad (7)$$

55 where  $q_{surf}$  is the surface energy flux in  $[W\ m^{-2}]$ ;  $q_{SW}$  is the net shortwave radiation;  $q_{LW}$  is the net  
 56 longwave radiation;  $q_L$  and  $q_S$  are the turbulent latent and sensible heat fluxes.  $q_F$  represents the heat  
 57 exchange of the fountain water droplets with the AIR ice surface.  $q_G$  represents ground heat flux between  
 58 Icestupa surface and Icestupa interior. Energy transferred in the direction of the ice surface is always  
 59 denoted as positive and away as negative.

60 Equation 7 is usually referred to as the energy budget for “the surface”, but practically it must apply  
 61 to a surface layer of ice with a finite thickness  $\Delta x$ . The energy flux acts upon the Icestupa surface layer  
 62 which has an upper and a lower boundary defined by the atmosphere and the ice body of the Icestupa,  
 63 respectively. The parameter selection for  $\Delta x$  is based on the following two arguments: (a) the ice thickness  
 64  $\Delta x$  should be small enough to represent the surface temperature variations every model time step  $\Delta t$  and  
 65 (b)  $\Delta x$  should be large enough for these temperature variations to not reach the bottom of the surface layer.  
 66 Therefore, we introduced a 20 mm thick surface layer for a model time step of 1 hour, over which the  
 67 energy balance is calculated. A sensitivity analysis was later performed to understand the influence of this  
 68 factor. Here, we define the surface temperature  $T_{ice}$  to be the modelled average temperature of the Icestupa  
 69 surface layer and the energy flux  $q_{surf}$  is assumed to act uniformly across the Icestupa area  $A$ .

### 70 2.2.1 Net Shortwave Radiation $q_{SW}$

71 The net shortwave radiation  $q_{SW}$  is computed as follows:

$$q_{SW} = (1 - \alpha) \cdot (SW_{direct} \cdot f_{cone} + SW_{diffuse}) \quad (8)$$

72 where  $SW_{direct}$  and  $SW_{diffuse}$  are the ERA5 direct and diffuse short wave radiation,  $\alpha$  is the modelled  
 73 albedo and  $f_{cone}$  is the area fraction of the ice structure exposed to the direct shortwave radiation.

74 We model the albedo using a scheme described in Oerlemans and Knap (1998). The scheme records the  
 75 decay of albedo with time after fresh snow is deposited on the surface.  $\delta t$  records the number of time steps  
 76 after the last snowfall event. After snowfall, albedo changes over a time step,  $\delta t$ , as

$$\alpha = \alpha_{ice} + (\alpha_{snow} - \alpha_{ice}) \cdot e^{(-\delta t)/\tau} \quad (9)$$

77 where  $\alpha_{ice}$  is the bare ice albedo value (0.35),  $\alpha_{snow}$  is the snow ice albedo value (0.85) and  $\tau$  is a decay  
 78 rate, which determines how fast the albedo of the ageing snow reaches this value. The decay rate  $\tau$  is  
 79 assumed to have a base value of 10 days similar to values obtained by Schmidt et al. (2017) for wet surfaces  
 80 and its maximal value is set based on observations by Oerlemans and Knap (1998) as shown in Table 1.  
 81 Furthermore, the albedo  $\alpha$  varies depending on the water source that formed the current Icestupa surface.  
 82 Correspondingly, the albedo is reset to the value of bare ice albedo if the fountain is spraying water onto  
 83 the current ice surface and to the value of fresh snow albedo if a snowfall event occurred. Snowfall events  
 84 are assumed if the air temperature is below  $T_{ppt} = 1^{\circ}C$  (Fujita and Ageta, 2000).

85 The area fraction  $f_{cone}$  of the ice structure exposed to the direct shortwave radiation depends on the  
 86 shape considered. The direct solar radiation incident on the AIR surface is first decomposed into horizontal  
 87 and vertical components using the solar elevation angle  $\theta_{sun}$ . For a conical shape, half of the total curved  
 88 surface is exposed to the vertical component of the direct shortwave radiation and the projected triangle  
 89 of the curved surface is exposed to the horizontal component of the direct shortwave radiation. The solar

90 elevation angle  $\theta_{sun}$  used is modelled using the parametrisation proposed by Woolf (1968). Accordingly,  
 91  $f_{cone}$  is determined as follows:

$$f_{cone} = \frac{(0.5 \cdot r_{ice} \cdot h_{ice}) \cdot \cos\theta_{sun} + (\pi \cdot r_{ice}^2 / 2) \cdot \sin\theta_{sun}}{\pi \cdot r_{ice} \cdot (r_{ice}^2 + h_{ice}^2)^{1/2}} \quad (10)$$

92 The ERA5 diffuse shortwave radiation is assumed to impact the conical Icestupa surface uniformly.

### 93 2.2.2 Net Longwave Radiation $q_{LW}$

94 The net longwave radiation  $q_{LW}$  is determined as follows:

$$q_{LW} = LW_{in} - \sigma \cdot \epsilon_{ice} \cdot (T_{ice} + 273.15)^4 \quad (11)$$

95 where  $T_a$  represents the measured air temperature,  $T_{ice}$  is the modelled surface temperature, both  
 96 temperatures are given in  $^{\circ}\text{C}$ ,  $\sigma = 5.67 \cdot 10^{-8} \text{ J m}^{-2} \text{ s}^{-1} \text{ K}^{-4}$  is the Stefan-Boltzmann constant,  $LW_{in}$   
 97 denotes the incoming longwave radiation derived from the ERA5 dataset and  $\epsilon_{ice}$  is the corresponding  
 98 emissivity value for the Icestupa surface (see Table 1).

### 99 2.2.3 Turbulent sensible $q_S$ and latent $q_L$ heat fluxes

100 The turbulent sensible  $q_S$  and latent heat  $q_L$  fluxes are computed with the following expressions proposed  
 101 by Garratt (1992):

$$q_S = c_a \cdot \rho_a \cdot p_a / p_{0,a} \cdot \frac{\kappa^2 \cdot v_a \cdot (T_a - T_{ice})}{(\ln \frac{h_{AWS}}{z_{ice}})^2} \quad (12)$$

$$q_L = 0.623 \cdot L_s \cdot \rho_a / p_{0,a} \cdot \frac{\kappa^2 \cdot v_a (p_{v,a} - p_{v,ice})}{(\ln \frac{h_{AWS}}{z_{ice}})^2} \quad (13)$$

102 where  $h_{AWS}$  is the measurement height above the ground surface of the AWS (in  $m$ ),  $v_a$  is the wind  
 103 speed in  $[m s^{-1}]$ ,  $c_a$  is the specific heat of air at constant pressure ( $1010 \text{ J kg}^{-1} \text{ K}^{-1}$ ),  $\rho_a$  is the air density  
 104 at standard sea level ( $1.29 \text{ kg m}^{-3}$ ),  $p_{0,a}$  is the air pressure at standard sea level ( $1013 \text{ hPa}$ ),  $\kappa$  is the  
 105 von Karman constant (0.4),  $L_s$  is the heat of sublimation ( $2848 \text{ kJ kg}^{-1}$ ) and  $z_{ice}$  (1.7 mm) denotes the  
 106 roughness length of ice (momentum and scalar). The vapor pressures over air ( $p_{v,a}$ ) and ice ( $p_{v,ice}$ ) was  
 107 obtained using the following formulation given in WMO (2018):

$$p_{v,a} = 6.107 \cdot 10^{(7.5 \cdot T_a / (T_a + 237.3))} \\ p_{v,ice} = (1.0016 + 3.15 \cdot 10^{-6} \cdot p_a - 0.074 \cdot p_a^{-1}) \cdot (6.112 \cdot e^{(22.46 \cdot T_{ice} / (T_{ice} + 272.62))}) \quad (14)$$

108 where  $p_a$  is the measured air pressure in [ $\text{hPa}$ ].

### 109 2.2.4 Fountain water heat flux $q_F$

110 The interaction between the fountain water and the ice surface is taken into account by assuming that  
 111 the ice surface temperature remains constant at  $0^{\circ}\text{C}$  during time steps when the fountain is active. This  
 112 process can be divided into two simultaneous steps: (a) the water temperature  $T_{water}$  is cooled to  $0^{\circ}\text{C}$

113 and (b) the ice surface temperature is warmed to  $0^{\circ}\text{C}$ . Process (a) transfers the necessary energy for  
 114 process (b) throughout the fountain runtime. We further assume that this process is instantaneous, i.e. the  
 115 ice temperature is immediately set to  $0^{\circ}\text{C}$  within just one time step  $\Delta t$  when the fountain is switched on.  
 116 Thus, the heat flux caused by the fountain water is calculated as follows:

$$q_F = \begin{cases} 0 & \text{if } \Delta M_F = 0 \\ \frac{\Delta M_F \cdot c_{water} \cdot T_{water}}{\Delta t \cdot A} + \frac{\rho_{ice} \cdot \Delta x \cdot c_{ice} \cdot T_{ice}}{\Delta t} & \text{if } \Delta M_F > 0 \end{cases} \quad (15)$$

117 with  $c_{ice}$  as the specific heat of ice.

#### 118 2.2.5 Bulk Icestupa heat flux $q_G$

119 The bulk Icestupa heat flux  $q_G$  corresponds to the ground heat flux in normal soils and is caused by the  
 120 temperature gradient between the surface layer ( $T_{ice}$ ) and the ice body ( $T_{bulk}$ ). It is expressed by using the  
 121 heat conduction equation as follows:

$$q_G = k_{ice} \cdot (T_{bulk} - T_{ice}) / l_{ice} \quad (16)$$

122 where  $k_{ice}$  is the thermal conductivity of ice ( $2.123 \text{ W m}^{-1} \text{ K}^{-1}$ ),  $T_{bulk}$  is the mean temperature of the  
 123 ice body within the Icestupa and  $l_{ice}$  is the average distance of any point in the surface to any other point in  
 124 the ice body.  $T_{bulk}$  is initialised as  $0^{\circ}\text{C}$  and later determined from Eqn. 16 as follows:

$$T_{bulk}^{i+1} = T_{bulk} - (q_G \cdot A \cdot \Delta t) / (M_{ice} \cdot c_{ice}) \quad (17)$$

125 Since AIR's typically have conical shapes with  $r_{ice} \gg h_{ice}$ , we assume that the center of mass of the ice  
 126 body is near the base of the fountain. Thus, the distance of every point in the AIR surface layer from the ice  
 127 body's center of mass is between  $h_{ice}$  and  $r_{ice}$ . So we calculate  $q_G$  here assuming  $l_{ice} = (r_{ice} + h_{ice})/2$ .

### 128 2.3 Surface temperature

129 The available energy  $q_{surf}$  can act on the surface of the AIR to a) change its temperature, b) melt ice or  
 130 c) freeze ice. So Eqn. 7 can be rewritten as:

$$q_{surf} = q_{freeze/melt} + q_T \quad (18)$$

131 where  $q_T$ ,  $q_{freeze}$  and  $q_{melt}$  represent energy associated with process (a), (b) and (c) respectively.

132 To distribute the surface energy flux into these three components, we categorize the model time steps  
 133 as freezing or melting events. Freezing events can only occur if there is fountain water available and the  
 134 surface energy flux is negative. But just these two conditions are not sufficient as the latent heat energy  
 135 can only contribute to temperature fluctuations. So to prevent latent heat energy from turning a melting  
 136 event into a freezing event an additional condition namely  $(q_{surf} - q_L) < 0$  is required. Thus, freezing and  
 137 melting events are identified as follows:

$$q_{freeze/melt} = \begin{cases} q_{freeze} & \text{if } \Delta M_F > 0 \text{ and } q_{surf} < 0 \text{ and } (q_{surf} - q_L) < 0 \\ q_{melt} & \text{otherwise} \end{cases} \quad (19)$$

138 During a freezing event, the available energy  $(q_{surf} - q_L)$  can either be sufficient or insufficient to  
 139 freeze the fountain water available. If insufficient, the additional energy further cools down the surface  
 140 temperature. So the surface energy flux distribution during a freezing event can be represented as:

**Table 1.** Free parameters in the model categorised as constant, uncertain and site parameters. Base value (B) and uncertainty (U) were taken from the literature. For assumptions (assum.), the uncertainty was chosen to be relatively large (5 %). For measurements (meas.), the uncertainty due to parallax errors is chosen to be (1 %).

Constant Parameters	Symbol	Value	References
Van Karman constant	$\kappa$	0.4	B: Cuffey and Paterson
Stefan Boltzmann constant	$\sigma$	$5.67 \cdot 10^{-8} W m^{-2} K^{-4}$	B: Cuffey and Paterson
Air pressure at sea level	$p_{0,a}$	1013 hPa	B: Mölg and Hardy
Density of water	$\rho_w$	$1000 kg m^{-3}$	B: Cuffey and Paterson
Density of ice	$\rho_{ice}$	$917 kg m^{-3}$	B: Cuffey and Paterson
Density of air	$\rho_a$	$1.29 kg m^{-3}$	B: Mölg and Hardy
Specific heat of ice	$c_{ice}$	$2097 J kg^{-1} ^\circ C^{-1}$	B: Cuffey and Paterson
Specific heat of water	$c_w$	$4186 J kg^{-1} ^\circ C^{-1}$	B: Cuffey and Paterson
Specific heat of air	$c_a$	$1010 J kg^{-1} ^\circ C^{-1}$	B: Mölg and Hardy
Thermal conductivity of ice	$k_{ice}$	$2.123 W m^{-1} K^{-1}$	B: Bonales et al.
Latent Heat of Sublimation	$L_s$	$2848 kJ kg^{-1}$	B: Cuffey and Paterson
Latent Heat of Fusion	$L_f$	$334 kJ kg^{-1}$	B: Cuffey and Paterson
Uncertain Parameters		Range	
Precipitation	$T_{ppt}$	$1 ^\circ C$	$\pm 1 ^\circ C$
Temperature threshold			B + U: Fujita and Ageta, Zhou et al.
Ice Emissivity	$\epsilon_{ice}$	0.95	[0.949,0.993]
Ice Albedo	$\alpha_{ice}$	0.35	$\pm 5 \%$
Snow Albedo	$\alpha_{snow}$	0.85	$\pm 5 \%$
Albedo Decay Rate	$\tau$	10 days	[1, 22] days
Surface layer thickness	$\Delta x$	20 mm	[1, 10] mm
Fountain Parameters		Range	
Spray Radius	$r_{spray}$		$\pm 5 \%$
Water temperature	$T_{water}$	$1 ^\circ C$	[0, 5] $^\circ C$

$$(q_{freeze}, q_T) = \begin{cases} (q_{surf} - q_L, q_L) & \text{if } \Delta M_F \geq -\frac{(q_{surf} - q_L)A \cdot \Delta t}{L_f} \\ (\frac{\Delta M_F \cdot L_f}{A \cdot \Delta t}, q_{surf} + \frac{\Delta M_F \cdot L_f}{A \cdot \Delta t}) & \text{if } \Delta M_F < -\frac{(q_{surf} - q_L)A \cdot \Delta t}{L_f} \end{cases} \quad (20)$$

141 During a melting event, the surface energy flux ( $q_{surf}$ ) is first used to change the surface temperature to  
 142  $T_{temp}$  calculated as:

$$T_{temp} = \frac{q_{surf} \cdot \Delta t}{\rho_{ice} \cdot c_{ice} \cdot \Delta x} + T_{ice} \quad (21)$$

143 If  $T_{temp} > 0^\circ C$ , then energy is reallocated from  $q_T$  to  $q_{melt}$  to maintain surface temperature at melting  
 144 point. So the surface energy flux distribution during a melting event can be represented as:

$$(q_{melt}, q_T) = \begin{cases} (0, q_{surf}) & \text{if } T_{temp} < 0 \\ \left(\frac{T_{temp} \cdot \rho_{ice} \cdot c_{ice} \cdot \Delta x}{\Delta t}, q_{surf} - \frac{T_{temp} \cdot \rho_{ice} \cdot c_{ice} \cdot \Delta x}{\Delta t}\right) & \text{if } T_{temp} > 0 \end{cases} \quad (22)$$

## 145 2.4 Mass Balance

146 The mass balance equation for an AIR is represented as:

$$\frac{\Delta M_F + \Delta M_{ppt} + \Delta M_{dep}}{\Delta t} = \frac{\Delta M_{ice} + \Delta M_{water} + \Delta M_{sub} + \Delta M_{runoff}}{\Delta t} \quad (23)$$

147 where  $M_F$  is the discharge of the fountain;  $M_{ppt}$  is the cumulative precipitation;  $M_{dep}$  is the cumulative  
 148 accumulation through water vapour deposition;  $M_{ice}$  is the cumulative mass of ice;  $M_{water}$  is the cumulative  
 149 mass of melt water;  $M_{sub}$  represents the cumulative water vapor loss by sublimation and  $M_{runoff}$  represents  
 150 the fountain discharge runoff that did not interact with the AIR. The LHS of equation 23 represents the rate  
 151 of mass input and the RHS represents the rate of mass output for an AIR.

152 Precipitation input is calculated as shown in equation 24a where  $\rho_w$  is the density of water (1000  
 153  $kg m^{-3}$ ),  $ppt$  is the measured precipitation rate in  $[m s^{-1}]$  and  $T_{ppt}$  is the temperature threshold below  
 154 which precipitation falls as snow. Here, snowfall events were identified using  $T_{ppt}$  as  $1^{\circ}C$ . Snow mass  
 155 input is calculated by assuming a uniform deposition over the entire circular footprint of the Icestupa.

156 The latent heat flux is used to estimate either the evaporation and condensation processes or sublimation  
 157 and deposition processes as shown in equation 24b. During time steps at which surface temperature is  
 158 below  $0^{\circ}C$  only sublimation and deposition can occur, but if the surface temperature reaches  $0^{\circ}C$ ,  
 159 evaporation and condensation can also occur. As the differentiation between evaporation and sublimation  
 160 (and condensation and deposition) when the air temperature reaches  $0^{\circ}C$  is challenging, we assume  
 161 that negative (positive) latent heat fluxes correspond only to sublimation (deposition), i.e. no evaporation  
 162 (condensation) is calculated.

163 Since we have categorized every time step as a freezing and melting event, we can determine the meltwater  
 164 and ice generated using the associated energy fluxes as shown in equations 24c and 24d. Having calculated  
 165 all the other mass components the fountain wastewater generated every time step can be calculated using  
 166 equation 24e.

$$\frac{\Delta M_{ppt}}{\Delta t} = \begin{cases} \pi \cdot r_{ice}^2 \cdot \rho_w \cdot ppt & \text{if } T_a < T_{ppt} \\ 0 & \text{if } T_a \geq T_{ppt} \end{cases} \quad (24a)$$

$$\left(\frac{\Delta M_{dep}}{\Delta t}, \frac{\Delta M_{sub}}{\Delta t}\right) = \begin{cases} \frac{q_L \cdot A}{L_s} \cdot (1, 0) & \text{if } q_L \geq 0 \\ \frac{q_L \cdot A}{L_s} \cdot (0, -1) & \text{if } q_L < 0 \end{cases} \quad (24b)$$

$$\frac{\Delta M_{water}}{\Delta t} = \frac{q_{melt} \cdot A}{L_f} \quad (24c)$$

$$\frac{\Delta M_{ice}}{\Delta t} = \frac{q_{freeze} \cdot A}{L_f} + \frac{\Delta M_{ppt}}{\Delta t} + \frac{\Delta M_{dep}}{\Delta t} - \frac{\Delta M_{sub}}{\Delta t} - \frac{\Delta M_{melt}}{\Delta t} \quad (24d)$$

$$\frac{\Delta M_{runoff}}{\Delta t} = \frac{\Delta M_F - \Delta M_{ice}}{\Delta t} \quad (24e)$$

**Table 2.** Summary of mass balance components for the EP experiment after the fountain spray was stopped (on 15<sup>th</sup> February 2019) and at the end of the model run (on 5<sup>th</sup> April). All parameters except  $M_F$  were modelled.

	Mass Component	Fountain spray ends	Model ends
Input	$M_F$	18060 kg	18060 kg
	$M_{ppt}$	444 kg	466 kg
	$M_{dpt}$	0 kg	0 kg
	$M_{cdt}$	7 kg	32 kg
Output	$M_{water}$	163 kg	1013 kg
	$M_{ice}$	809 kg	0 kg
	$M_{vapour}$ $M_{runoff}$	11 kg 17529 kg	16 kg 17529 kg

167 Considering AIRs as water reservoirs, we can quantify their potential through the amount of water they  
 168 store (storage quantity) and the length of time they store it (storage duration). Another means of comparing  
 169 different Icestupas is through their water storage efficiency defined accordingly as:

$$\text{Storage Efficiency} = \frac{M_{water}}{(M_F + M_{ppt} + M_{dep})} \cdot 100 \quad (25)$$

### 3 MODEL RESULTS

170 The model was forced with meteorological data from 30<sup>th</sup> January to 5<sup>th</sup> April 2019 (Fig. 1) and various  
 171 parameters (see Table 1) to calculate the mass and energy balance of the Icestupa.

#### 172 3.1 Energy and mass balance calculation

173 Daily averages of some components of the energy balance are shown in Fig. 2 (b). On average during  
 174 the experiment duration, the total energy balance was almost zero. Net shortwave radiation ( $33 \text{ Wm}^{-2}$ ),  
 175 sensible ( $10 \text{ Wm}^{-2}$ ) and latent heat flux ( $2 \text{ Wm}^{-2}$ ) with a mostly positive flux towards the surface of the  
 176 icestupa were compensated by the surf longwave radiation (-  $34 \text{ Wm}^{-2}$ ) and the melt energy (-  $12 \text{ Wm}^{-2}$ ).  
 177 The contributions of other fluxes were negligible in comparison.

178 Net shortwave radiation is the main input to, and the most varying energy flux on the ice surface. Its  
 179 variability is controlled by the surface albedo  $\alpha$  and the area fraction  $f_{cone}$  which therefore represent key  
 180 variables in the energy balance (Fig. ?? (b)). Although global radiation flux reached a daily maximum  
 181 value of  $339 \text{ Wm}^{-2}$ ,  $q_{SW}$  only went up to  $98 \text{ Wm}^{-2}$ . This is caused by the fact that only about 30 % of  
 182 the direct solar radiation influenced the Icestupa surface as shown by the area fraction  $f_{cone}$  in Fig. ?? (a).  
 183 Snowfall is the atmospheric variable connected most closely and proportionally to albedo. Higher and/or  
 184 more frequent snowfall thus decreases the energy available for melt due to the corresponding increase in  $\alpha$ .

185  $q_{LW}$  was predominantly negative indicating that this energy balance component drove the freezing of  
 186 the ice structure. Daily values of  $q_{LW}$  ranged from -89 to  $21 \text{ Wm}^{-2}$ . Turbulent sensible heat flux  $q_S$   
 187 contributed mostly to the melt of the ice structure. Daily values of  $q_S$  ranged from -14 to  $26 \text{ Wm}^{-2}$ .  
 188 Deposition/condensation was favored over evaporation/sublimation during 95 % of the model runtime.  
 189 Daily values of the turbulent latent heat flux  $q_L$  ranged from -10 to  $15 \text{ Wm}^{-2}$ . Since the mean of  $q_L$  was  
 190 positive, the Icestupa gained mass cumulatively from the atmosphere due to the condensation process.

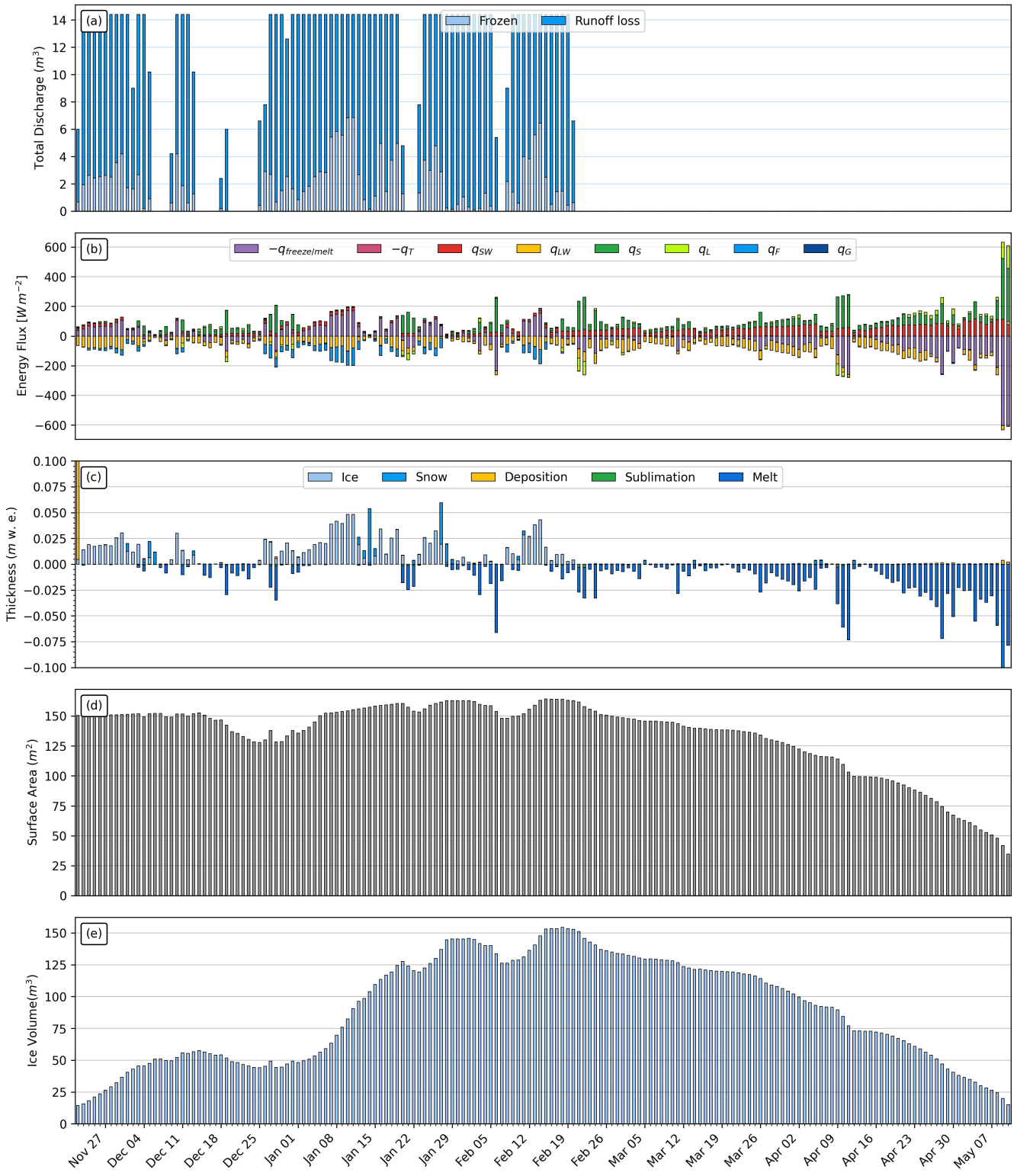


**Figure 2.** (a) Fountain discharge (b) energy flux components, (c) mass flux components (d) surface area and (e) volume of the Icestupa in daily time steps.  $q_{SW}$  is the net shortwave radiation;  $q_{LW}$  is the net longwave radiation;  $q_L$  and  $q_S$  are the turbulent latent and sensible heat fluxes.  $q_F$  represents the interactions of the fountain water with the AIR surface layer.  $q_G$  quantifies the heat conduction process between the AIR surface layer and the ice body.

191 Fountain water heat flux  $q_F$  had a mean of zero as it was only nonzero during 1002 time steps or around  
 192 100 hours. Daily values of  $q_F$  ranged from -1 to  $6 \text{ W m}^{-2}$ . The contribution of heat flux by conduction  
 193  $q_G$  was also minimal as it only varied between -6 to  $12 \text{ W m}^{-2}$  with a mean of  $0 \text{ W m}^{-2}$ . The energy  
 194 contributing to surface temperature changes ( $q_T$ ) was insignificant in comparison to the energy spent on  
 195 freezing and melting ( $q_{melt}$ ). The resulting bulk temperature and the surface temperature are shown in Fig.  
 196 ?? (b). For the total considered period,  $q_{LW}$  accounted for 33.8% of overall energy turnover. The energy  
 197 turnover is calculated as the sum of energy fluxes in absolute values.  $q_{SW}$  accounted for 31.3%, followed  
 198 by  $q_{melt}$  (19%),  $q_S$  (9.6%),  $q_L$  (3.6%),  $q_G$  (2.4%),  $q_F$  (0.2%) and  $q_T$  (0.4%).

199 Fig. 2 (c) represents the mass fluxes associated with these energy exchanges expressed in  $m$  w.e. It  
 200 shows the ice and meltwater formed due to  $q_{melt}$ , snow accumulated due to precipitation, water vapour  
 201 deposition/condensation and sublimation/evaporation due to  $q_L$ . Growth rate ( $\frac{\Delta M_{ice}}{\Delta t}$ ) shows a better  
 202 correlation with surf energy flux ( $r^2 = 0.15$ ) compared to Icestupa surface area ( $r^2 = 0.04$ ). This is  
 203 because the variance in growth rate is mostly due to the variance in  $q_{surf}$  as illustrated in Fig. 2. Since  $r_{ice}$   
 204 was initialised with the spray radius  $r_{spray}$ , the surface area maintains a maximum initially until the energy  
 205 flux becomes positive. This trend favours the positive over the negative thickness changes resulting in a  
 206 steep increase and gradual melting of ice volume as can be seen in Fig. 3.

207 The total water used for the Icestupa development includes contributions from the fountain (97.3%),  
 208 snowfall (2.5 %), condensation (0.2 %) as shown in Table 2. The maximum ice mass during the whole  
 209 measurement period was  $809 \text{ kg}$ , which occurred after the last fountain run on Feb 16<sup>th</sup> 2019 in the morning.  
 210 Therefore, in the case of EP we used a water input of  $18,558 \text{ kg}$ , with a resultant storage efficiency of only  
 211 5.5 %.

## REFERENCES

- 212 Bonales, L. J., Rodriguez, A. C., and Sanz, P. D. (2017). Thermal conductivity of ice prepared under  
 213 different conditions. *International Journal of Food Properties* 20, 610–619. doi:10.1080/10942912.  
 214 2017.1306551
- 215 [Dataset] Copernicus Climate Change Service (C3S) (2017). Era5: Fifth generation ecmwf atmospheric  
 216 reanalyses of the global climate. [Available at <https://cds.climate.copernicus.eu/cdsapp#!/home>, accessed 2019-10-01]
- 217 Cuffey, K. M. and Paterson, W. S. B. (2010). *The Physics Of Glaciers* (Elsevier)
- 218 Fujita, K. and Ageta, Y. (2000). Effect of summer accumulation on glacier mass balance on the  
 219 tibetan plateau revealed by mass-balance model. *Journal of Glaciology* 46, 244–252. doi:10.3189/  
 220 172756500781832945
- 221 Garratt, J. R. (1992). *The Atmospheric Boundary Layer* (Cambridge University Press)
- 222 Hock, R. (2005). Glacier melt: a review of processes and their modelling. *Progress in Physical Geography:  
 223 Earth and Environment* 29, 362–391
- 224 Hori, M., Aoki, T., Tanikawa, T., Motoyoshi, H., Hachikubo, A., Sugiura, K., et al. (2006). In-situ  
 225 measured spectral directional emissivity of snow and ice in the 8–14 micrometer atmospheric window.  
 226 *Remote Sensing of Environment* 100, 486 – 502
- 227 Meteoblue (2020). Climate schwarzsee [Available at [https://www.meteoblue.com/en/weather/historyclimate/climatemodeled/schwarzsee\\_switzerland\\_11790334](https://www.meteoblue.com/en/weather/historyclimate/climatemodeled/schwarzsee_switzerland_11790334), accessed 2019-10-01]
- 228 Mölg, T. and Hardy, D. R. (2004). Ablation and associated energy balance of a horizontal glacier surface  
 229 on kilimanjaro. *J. Geophys. Res.-Atmos.* 109, 1–13. doi:10.1029/2003JD004338

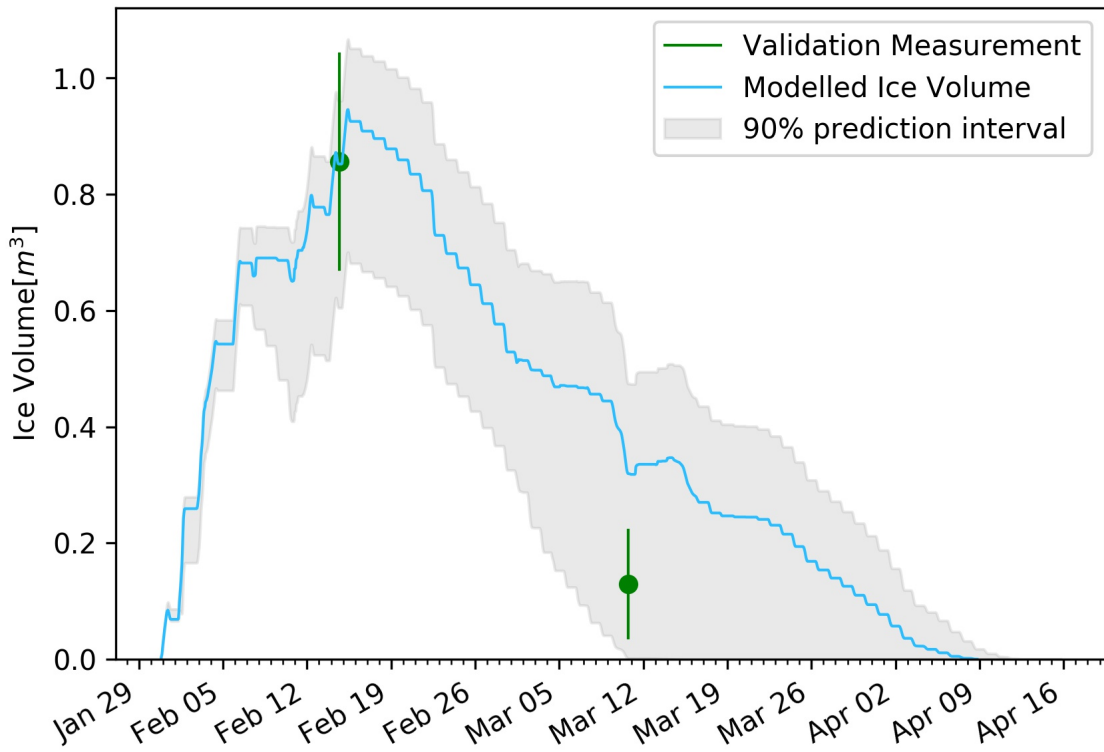


**Figure 3.** Modelled ice volume during the lifetime of the EP Icestupa (blue curve). Green line segments indicate the first and second validation measurements. The prediction interval is based on the ice volume uncertainty caused by the most sensitive parameters, namely, temperature threshold below which precipitation falls as snow and the ice emissivity.

- 233 Oerlemans, J. and Knap, W. H. (1998). A 1 year record of global radiation and albedo in the  
234 ablation zone of morteratschgletscher, switzerland. *Journal of Glaciology* 44, 231–238. doi:10.  
235 3189/S0022143000002574
- 236 Scherrer, S. C. (2020). Temperature monitoring in mountain regions using reanalyses: lessons from the  
237 alps. *Environmental Research Letters* 15, 044005
- 238 Schmidt, L. S., Aðalgeirs Þóttir, G., Guðmundsson, S., Langen, P. L., Pálsson, F., Mottram, R., et al. (2017).  
239 The importance of accurate glacier albedo for estimates of surface mass balance on vatnajökull: evaluating  
240 the surface energy budget in a regional climate model with automatic weather station observations. *The  
241 Cryosphere* 11, 1665–1684. doi:10.5194/tc-11-1665-2017
- 242 WMO (2018). *Guide to Instruments and Methods of Observation* (World Meteorological Organization ;  
243 2018 (2018 Edition))
- 244 Woolf, H. M. (1968). *On the Computation of Solar Elevation Angles and the determination of sunrise and  
245 sunset times* (National Aeronautics and Space Administration)
- 246 Zhou, S., Kang, S., Gao, T., and Zhang, G. (2010). Response of zhadang glacier runoff in nam co basin,  
247 tibet, to changes in air temperature and precipitation form. *Chinese Science Bulletin* 55, 2103–2110.  
248 doi:10.1007/s11434-010-3290-5